ACS OMEGA

http://pubs.acs.org/journal/acsodf

Article

Fe–Fe_3C Functionalized Few-Layer Graphene Sheet Nanocomposites for an Efficient Electrocatalyst of the Oxygen Reduction Reaction

Meiling Sun, Fangying Yuan, Runqiu Li, Shijun Dong, Ye Zhao, Wenxia Zhong, Chang Shen, Junpeng Wu, and Hui Zheng*

Cite This: *ACS Omega* 2022, 7, 25458–25465

Read Online

ACCESS | Metrics & More | Article Recommendations

ABSTRACT: Preparation of a high-efficiency, low-cost, and environmentally friendly non-precious metal catalyst for the oxygen reduction reaction (ORR) is highly desirable in fuel cells. Herein, a Fe–Fe_3C-functionalized few-layer graphene sheet (Fe/Fe_3C/FLG) nanocomposite was fabricated through the vacuum heat treatment technique using ferric nitrate and glucose as the precursors and exhibited a high-performance ORR electrocatalyst. Multiple characterizations confirm that the nanosized Fe particles with the Fe_3C interface are uniformly distributed in the FLGs. Electrocatalytic kinetics investigation of the nanocomposite indicates that the electron transfer process is a four-electron pathway. The formation of the Fe_3C interface between the Fe nanoparticles and FLGs may promote the electron transfer from the Fe to FLGs. Furthermore, the Fe/Fe_3C/FLG nanocomposite not only exhibits high ORR catalytic activity but also displays desirable stability. Consequently, the obtained Fe/Fe_3C/FLG nanocomposite might be a promising non-precious, cheap, and high-efficiency catalyst for fuel cells.

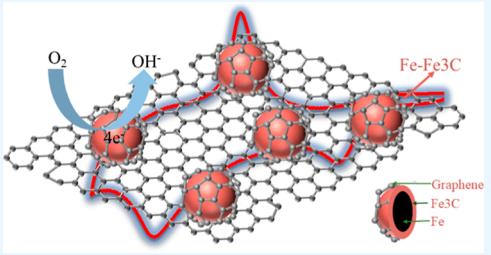

1. INTRODUCTION

With the growing demand for fossil fuels and increasing environmental problems from burning fossil fuels, searching for clean and reproducible energies has become a hotspot for research. Meanwhile, the fuel cell has been considered the best candidate for high energy density and environmentally friendly energy storage conversion devices.[1,2] Fuels react with oxygen by mild electrochemical processes without combustion and the overall fuel-conversion efficiency is not limited by the Carnot cycle law.[3] The ORR is a crucial reaction that happens at the cathode during the electrochemical process of energy conversion.[4,5] Nevertheless, due to the sluggish reaction process for the large energy barrier, a highly active catalyst is required to promote the reduction reaction.[6,7]

Nowadays, Pt and Pt-based materials are considered the most reliable ORR electrocatalysts.[8] However, the high cost and element scarcity of Pt impede the practical application of fuel cells.[9] To address this issue, it is meaningful that the electrodes for future fuel cells will be free of Pt and Pt-based materials. Therefore, the preparation of a high-efficiency, low-cost, and environmentally friendly non-precious metal catalyst for ORR is highly desirable in fuel cells. Among the metals, the Fe, Co, and Mn have been extensively studied for their cheapness and plentifulness.[10−12] Furthermore, the Fe-based catalyst possesses the highest ORR activity (Fe > Co > Mn).[13,14] The special electron orbital structure of the Fe-based catalyst is easily modified by using inorganic coordination structures to improve the adsorption of oxygen on the catalyst surface, resulting in high catalytic activity and desirable stability.[14] However, the iron-only catalyst is still insufficient mainly because of the aggregation of metal atoms and the poor control of the distribution, interfering with the dispersion of active sites and limiting the catalytic durability and efficiency.[15,16]

Recent studies show that graphene, as a strictly two-dimensional material, has evoked extensive interest for its abundant physical properties, such as high electrical conductivity, high electron mobility, good structure flexibility, and large surface area (2630 m^2/g).[17−20] Therefore, graphene has been considered an ideal substrate that provides a good platform for the dispersion of metal nanoparticles.[21−24] Numerous metal nanoparticles have been attempted to deposit on the graphene and studied its catalytic performance. A crucial issue is to deal well with the interface between graphene and metal nanoparticle, which directly influences the electron transfer process. Many research works had shown that the FeN, Fe_3C, and FeP in catalysts as the modification were directly related to the ORR

Received: April 17, 2022
Accepted: June 30, 2022
Published: July 13, 2022

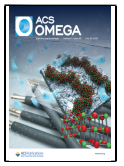

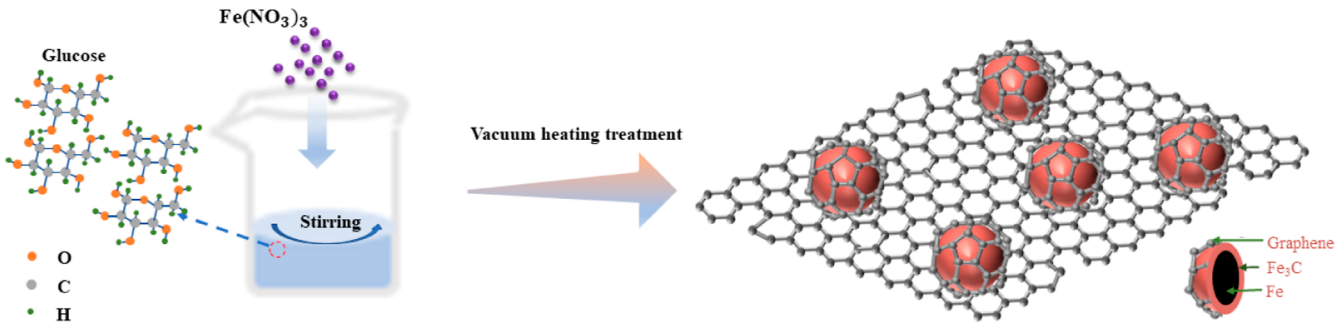

Figure 1. Schematic illustration of the synthesis procedure for the $Fe/Fe_3C/FLG$ nanocomposite.

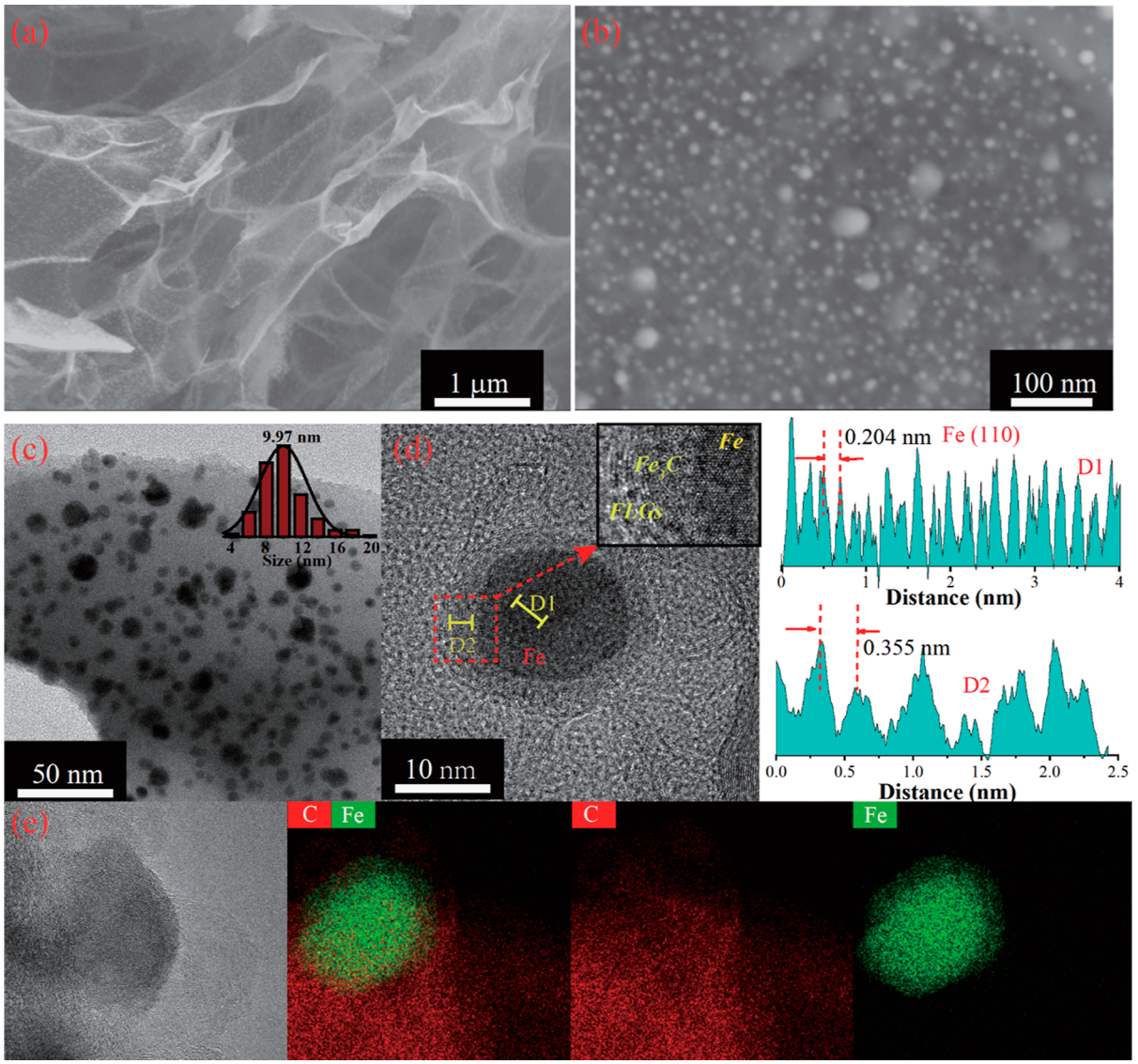

Figure 2. Morphology and microstructure of the $Fe/Fe_3C/FLG$ nanocomposite. (a) Low magnification of the FESEM image; (b) high magnification of the FESEM image; (c) low resolution of TEM, the inset is the size distribution of Fe particles; and (d) high resolution of TEM, the inset is the selected area magnification. The skeleton map of the selected position (D_1 and D_2) was also inserted in the right of (d); (e) EDS mapping of the corresponding C and Fe.

performance, which could further facilitate faster electron transfer.[25−30] The encapsulation of metal−metal carbide nanoparticles in the graphene layer activates the structure electrochemically toward ORR by reducing the work function of the carbon layer.[31]

In this work, we synthesized a non-precious, cheap, and high-efficiency $Fe/Fe_3C/FLG$ nanocomposite by using ferric nitrate and glucose as precursors, which exhibits a high-performance ORR electrocatalyst. The crystal structure, microstructure, and morphology of the as-synthesized $Fe/Fe_3C/FLG$ nanocompo-

https://doi.org/10.1021/acsomega.2c02395
ACS Omega 2022, 7, 25458−25465

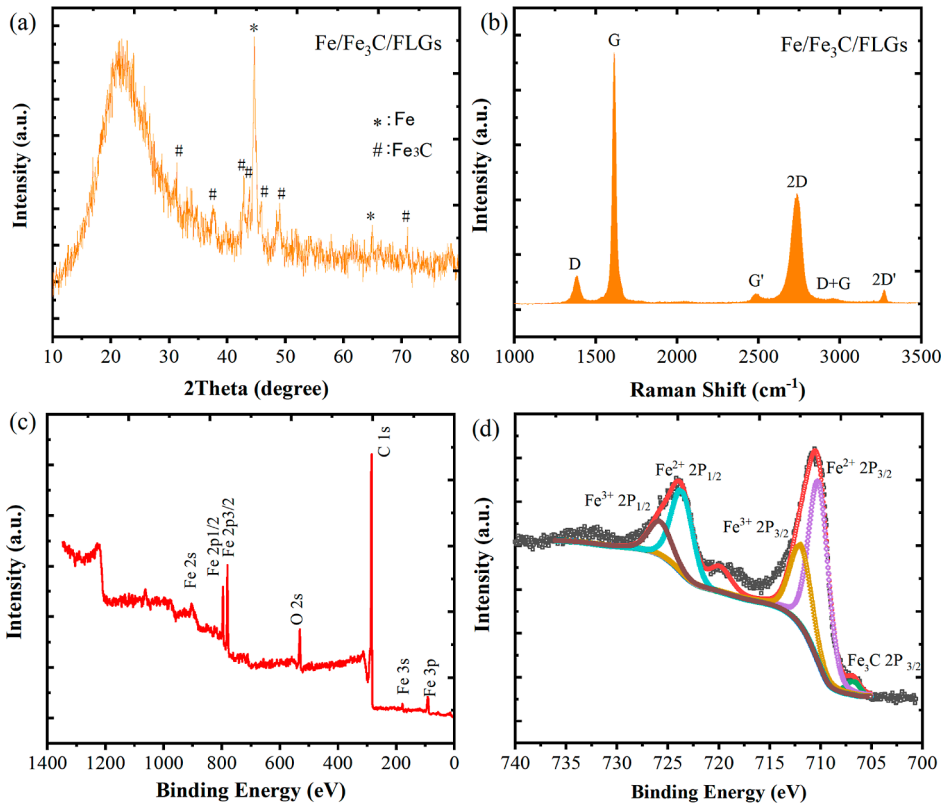

Figure 3. Crystal structure, chemical states, and composition of the Fe/Fe_3C/FLG nanocomposite. (a) XRD pattern; (b) Raman spectrum; (c) XPS spectrum; and (d) high-resolution Fe 2p spectrum.

site were extensively investigated. Additionally, the ORR performance and stability of the nanocomposite were also studied. The synthesized Fe/Fe_3C/FLG nanocomposite was demonstrated to be an excellent electrocatalyst for ORR.

2. MATERIALS AND METHODS

2.1. Preparation of the Fe/Fe_3C/FLG Nanocomposite. The Fe/Fe_3C/FLG nanocomposite was synthesized by using ferric nitrate and glucose as precursors. The schematic illustration of the synthesis procedure for the Fe/Fe_3C/FLG nanocomposite is shown in Figure 1. First, the solution containing ferric nitrate [reagent grade, $Fe(NO_3)_3 \geq 99.8\%$] and glucose (reagent grade, glucose $\geq 99.8\%$) was mixed. The concentration of Fe ions and glucose in the mixed solution is 0.01 and 0.05 M, respectively. After that, 500 μL of the prepared solution was spin-coated onto a quartz sheet with a rotating speed of 3000 r/s, followed by baking lamp drying for 24 h. Finally, the dried film was placed in the crucible and put into the tube furnace, and heated at 1000 °C for 0.5 h. Before heating, the furnace was pumped to 5×10^{-4} Pa, and then, the temperature increased to 1000 °C at a rate of 5 °C/min. After the heating, the furnace was allowed to cool down naturally to room temperature.

2.2. Characterization Technique. The as-synthesized Fe/Fe_3C/FLGs nanocomposite was characterized by multiple characterization tools. The surface morphology of Fe/Fe_3C/FLGs was examined by a field emission scanning electron microscope (JEOL 7600F). Transmission electron microscopy (TEM), elemental mapping, and high-resolution TEM (HRTEM) were performed on a JEOL-JEM2100 microscope to examine the morphologies, components, and microstructures of the Fe/Fe_3C nanoparticles. The crystal structure of the nanocomposite was analyzed by Raman scattering spectra of Renishaw confocal Raman spectroscopy with 10 MW output power (excitation wavelength used was 514 nm, Renishaw, Gloucestershire, gl127 DW) and X-ray diffraction (XRD, Rigaku IV). For the chemical composition and bonding state, X-ray photoelectron spectroscopy (XPS) was taken with Thermo Avantage ESCALAB 250 Xi instrument. The Brunauer–Emmett–Teller (BET) surface area was acquired using the ASAP2020 type nitrogen adsorption apparatus (micromeritics, USA).

2.3. Electrochemical Behavior Study. The electrochemical characterization of the Fe/Fe_3C/FLG nanocomposite was performed by the cyclic voltammetry (CV) and rotating disk electrode (RDE) voltammetry and rotating ring disk electrode (RRDE) (CHI instrument 760E, USA) with a traditional three-electrode setup comprising electrocatalysts modified glassy carbon electrode (GCE), Pt-wire, and Ag/AgCl as working, counter, and reference electrode, respectively, in an alkaline aqueous solution. In addition, the Fe/Fe_3C/FLG catalyst ink was prepared by mixing 2 mg of Fe/Fe_3C/FLGs and 40 μL of 5 wt % Nafion solution with 660 μL of deionized water followed by 45 min of sonication. From the catalyst ink, 8 μL was pipetted on GCE for electrochemical studies. Then, it was dried naturally at room temperature.

The electrolyte solution which was 0.1 M NaOH in our study was bubbled continuously with Ar for 30 min before electrochemical measurements. CV was performed at 50 mV·s^{-1} in either Ar- or O_2-saturated 0.1 M NaOH solution in a potential window of −1.2 to +0.2 V versus Ag/AgCl. Then, a constant O_2 flow over the 0.1 M NaOH instead of Ar was maintained during the measurement to ensure O_2 saturation of the solution. The linear sweep voltammetry (LSV) was

https://doi.org/10.1021/acsomega.2c02395
ACS Omega 2022, 7, 25458−25465

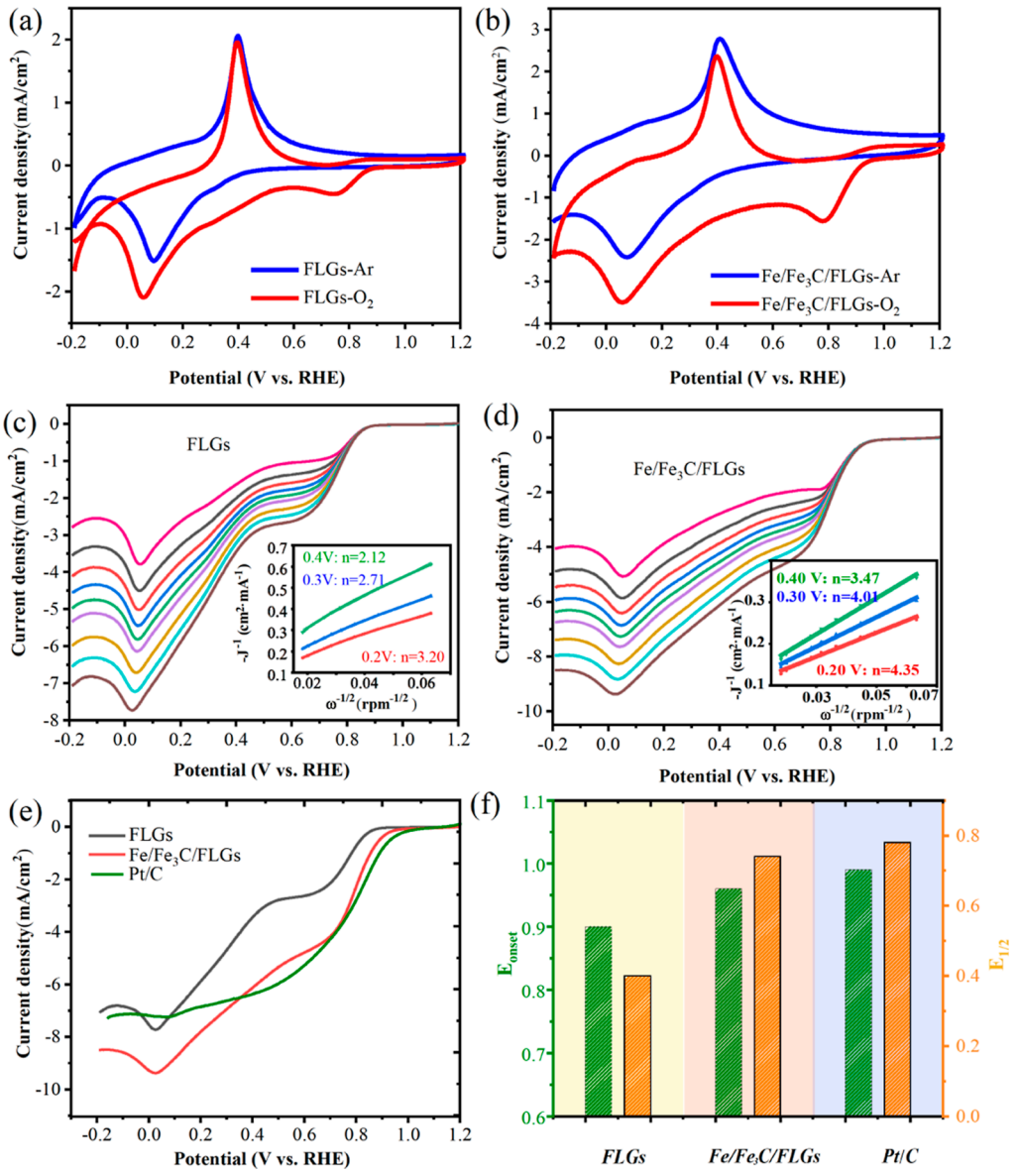

Figure 4. ORR performance of the $Fe/Fe_3C/FLGs$ and FLG materials. (a,b) CV curves of FLGs and $Fe/Fe_3C/FLGs$ in Ar-saturated and O_2-saturated 0.1 M NaOH solution. (c,d) LSV of FLGs and $Fe/Fe_3C/FLGs$ in O_2-saturated 0.1 M NaOH aqueous solution recorded at various rotation rates (250−3000 rpm), the insets are K−L plots and electron transfer number. j is the current density and ω is the angular velocity. (e) LSV curves at 3000 rpm of FLGs, Fe/Fe3C/FLGs, and Pt/C; (f) E_{onset} and $E_{1/2}$ of FLGs, $Fe/Fe_3C/FLGs$, and Pt/C.

measured in an oxygen-saturated 0.1 M NaOH aqueous solution from 0.2 to −1.2 V versus Ag/AgCl at a speed of 250−3000 rpm and a sweep rate of 10 $mV{\cdot}s^{-1}$. Besides, the hydrogen peroxide yield (H_2O_2 %) and the electron transfer number (n) were measured through RRDE at a speed of 10 $mV{\cdot}s^{-1}$ and the ring electrode potential was set to 1.20 V versus RHE. Electrochemical impedance spectroscopy (EIS) was performed in the frequency range from 1 MHz to 10 mHz with a voltage amplitude of 5 mV. The accelerated stability test was conducted between −1.2 and +0.2 V for 1000 cycles. The resistance to methanol poisoning tests was carried out by adding 2 mL of 0.5 M methanol at 500 s during the response.

3. RESULTS AND DISCUSSION

First, the morphology and microstructure of the $Fe/Fe_3C/FLG$ nanocomposite were characterized by field emission scanning electron microscopy (FESEM) and TEM, as shown in Figure 2. It is obvious from the low-magnification FESEM (in Figure 2a) that a nice lamellar graphene structure with crumpled flaky wrinkles is presented, in which the nanosized Fe particles are evenly dispersed. The transparent appearance indicates that graphene has few layers and high crystallinity. The high magnification image in Figure 2b sees that spherical Fe particles have a uniform grain size and distribution along with a few agglomerated large particles and are firmly embedded in the graphene sheets. BET analysis was performed, and the results show that the $Fe/Fe_3C/FLGs$ nanocomposite possessed a specific surface area of 116 $m^2\ g^{-1}$.

The TEM image in Figure 2c further shows that the spherical Fe particles are uniformly dispersed on graphene sheets. The histogram in the inset of Figure 2c gives the size distribution of Fe particles and presents a Gaussian distribution with an average diameter of 9.97 nm. The HRTEM image in Figure 2d displays that spherical Fe nanoparticles are coated with graphene sheets.

https://doi.org/10.1021/acsomega.2c02395
ACS Omega 2022, 7, 25458−25465

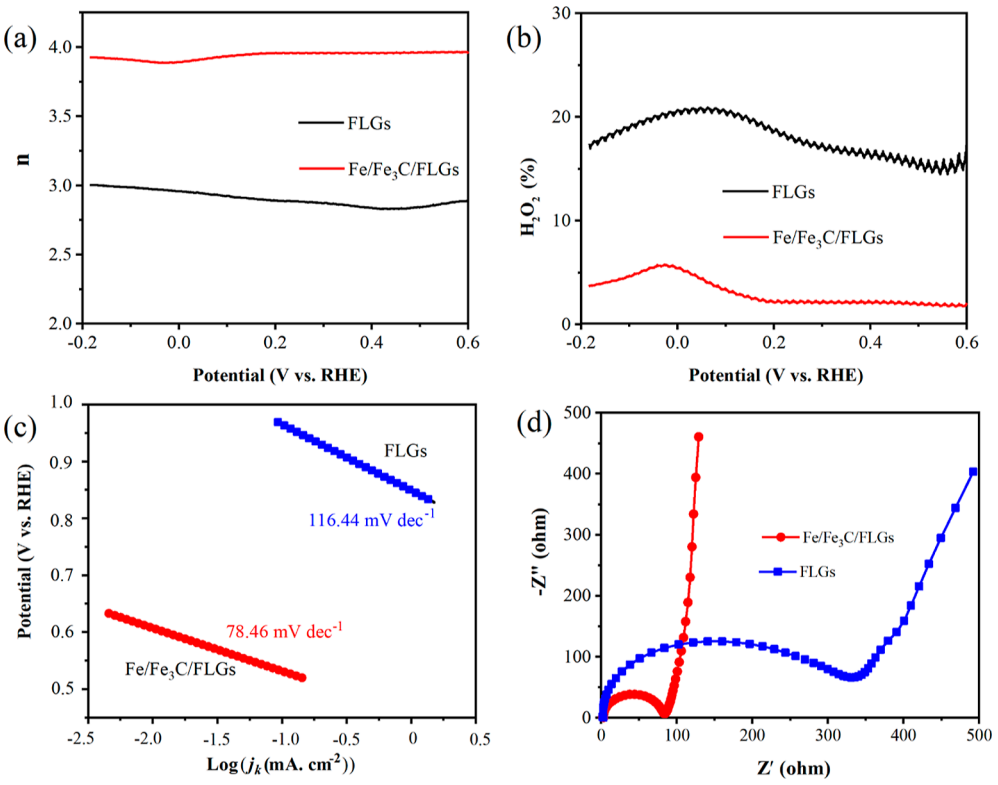

Figure 5. ORR performance of the $Fe/Fe_3C/FLGs$ and FLG materials. (a) Electron transfer number n vs potential; (b) H_2O_2 yield versus potential; (c) Tafel plots; and (d) EIS plots.

The line profile of the selected area is also given on the right of Figure 2d. The lattice spacing of the Fe crystallinity particles was measured to be 0.204 nm, corresponding to the Fe(110) basal plane. Meanwhile, the number of graphene layers was calculated to be about 6 from the number of peaks, and the lattice spacing is 0.355 nm which agrees with the theoretical plane spacing of graphene (0.35 nm). Furthermore, an obvious interface with 2 nm thickness is observed between the Fe particle and graphene, which is confirmed to be Fe_3C through the structural characterization. The mapping of constituent elements as shown in Figure 2f, which displays an interface region that contains Fe and C atoms is observed, which further confirms that the Fe_3C phase is formed in the interface between the Fe and graphene. The interface of Fe_3C can effectively contribute to the electron transfer between the graphene and Fe particles, which is beneficial to the ORR characteristics.

The crystal structure and chemical composition of the $Fe/Fe_3C/FLGs$ nanocomposite were further examined by XRD, Raman spectrometers, and XPS. The XRD pattern in Figure 3a shows characteristic peaks of Fe and Fe_3C, which indicate that the synthesized substance contains metallic Fe and Fe_3C, while no other phases. The disappearance of oxygen atoms in the substance can be explained as the C atom in graphene easily capturing the oxygen and reacting to CO_2 or CO gases. The amorphous envelope on the left of the pattern comes from the glass slide.

The Raman spectra of $Fe/Fe_3C/FLGs$ in Figure 3b exhibits six distinct peaks (D, G, G′, 2D, D + G, and 2D′ band). The shape of the characteristic 2D peak depends on the number of graphene layers, and the narrow and high envelope shape of the peak indicates the existence of a few layers of graphene in the prepared $Fe/Fe_3C/FLG$ composite, which is consistent with FESEM and TEM images. Additionally, the peak intensity ratio between D peak and G peak (I_D/I_G) displays the surface defect density in the graphene sheets.[27] The low value of I_D/I_G for the $Fe/Fe_3C/FLG$ composite indicates the low concentration of defects and the high crystallinity of graphene sheets.

The chemical states and composition of the $Fe/Fe_3C/FLG$ composite were characterized by XPS. Figure 3c shows the full XPS spectra of $Fe/Fe_3C/FLGs$ which exhibit three elements of Fe, O, and C. The peak of O 1s is speculated to come from the sample surface's adsorbed oxygen. The high-resolution Fe 2p spectrum displayed in Figure 3d is mainly composed of Fe^{3+} and Fe^{2+}, which is consistent with the general Fe spectrum. Especially, an inconspicuous peak appears at a binding energy of 706.5 eV, which corresponds to the 2p3/2 orbitals of Fe_3C.

The electrocatalytic activity and the ORR performance of the $Fe/Fe_3C/FLG$ nanocomposite were evaluated, in comparison with the FLGs and commercial Pt/C. The CV curves as seen in Figure 4a,b were conducted in 0.1 M NaOH solution with saturated Ar or O_2 at a voltage sweep rate of 50 mV/s, where the reduction peak was only observed in O_2. The oxygen reduction peak potential (E_{peak}) of FLGs and $Fe/Fe_3C/FLGs$ are located at 0.73 and 0.79 V, respectively. Figure 4c,d shows the LSV of FLGs and $Fe/Fe_3C/FLGs$ catalyst from 250 to 3000 r and also displays its Koutecky−Levich plots and electron transfer number. The polarization curves were obtained at the voltage from +1.2 to −0.2 V, which reveals an obvious increase in current density with the increase in the rotation rate because of the shortened diffusion layer distance.[32] In Figure 4c, a low current occurs between 0.5 and 0.7 V, followed by a second reduction wave at a lower positive potential, indicating that the ORR process of FLGs includes a two-electron path with hydrogen peroxide anion as the intermediate and then reduction to the hydroxyl anion. Koutechy−Levich (K−L) plots (insets of Figure 4c,d) show the first-order reaction kinetics of FLGs and

https://doi.org/10.1021/acsomega.2c02395
ACS Omega 2022, 7, 25458−25465

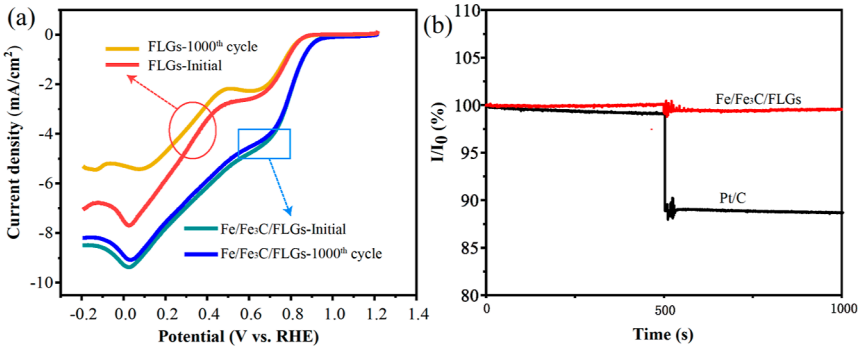

Figure 6. (a) Characterization of the durability of the FLGs and Fe/Fe_3C/FLG catalyst before and after 1000 potential cycles in O_2-saturated 0.1 M NaOH; (b) Resistance to methanol poisoning for Fe/Fe_3C/FLGs and Pt/C.

Fe/Fe_3C/FLGs with nearly parallel fitting lines reflecting the O_2 concentration, which also indicates a potential independent electron transfer rate. Moreover, the electron transfer number (n) of the ORR was determined using the K−L equations according to the K−L plots.[25] The n of Fe/Fe_3C/FLGs is between 3.47 and 4.35 in the voltage range of 0.2−0.4 V, while only 2.12−3.20 for FLGs. Therefore, the Fe/Fe_3C/FLG nanocomposite undergoes a four-electron pathway, while two-electron pathway for FLGs.

LSV curves of FLGs, Fe/Fe_3C/FLGs, and commercial Pt/C were measured in 0.1 M NaOH with O_2 saturated at a rotation rate of 3000 rpm and displayed in Figure 4e. The Fe/Fe_3C/FLGs composite shows the maximum limiting current density (~8.5 mA/cm^2) among the above three catalysts. Besides, the half-wave potential ($E_{1/2}$) of Fe/Fe_3C/FLGs is 0.74 V, which is higher than the FLGs (0.4 V) and comparable to Pt/C (0.78 V). Additionally, the onset potential (E_{onset}) is defined as the potential that is able to generate a current density of 0.1 mA/cm^2 during the ORR based on the recorded steady state polarization plots, which are located at 0.90, 0.96, and 0.99 V for FLGs, Fe/Fe_3C/FLGs, and Pt/C, respectively. To make a clear comparison, the E_{onset} and $E_{1/2}$ of FLGs, Fe/Fe_3C/FLGs, and Pt/C are also given in the histogram of Figure 4f, which are (0.90, 0.4 V), (0.96, 0.74 V), and (0.99, 0.78 V), respectively. Remarkably, the Fe/Fe_3C/FLG nanohybrid has a higher catalytic activity than FLGs and approaches to the commercial Pt/C electrode. The E_{onset} and $E_{1/2}$ of Fe/Fe_3C/FLGs are also higher than those of the reported Fe-rGO, Fe-NGM.[33−35] Therefore, Fe/Fe_3C/FLG composites are efficient non-precious metal ORR electrocatalysts, which have broad prospects for large-scale applications.

Furthermore, in order to detect the amount of intermediate H_2O_2 and obtain a more accurate electron transfer number during the ORR process, the RRDE measurements were performed in an oxygen saturated 0.1 M NaOH aqueous solution. The calculation of H_2O_2 % and n was deduced using the following eqs 1 and 2[36,37]

$$H_2O_2\ (\%) = 200 \times \frac{\frac{I_r}{N}}{\frac{I_r}{N} + I_d} \quad (1)$$

$$n = 4 \times \frac{I_d}{\frac{I_r}{N} + I_d} \quad (2)$$

where I_d and I_r are the disk and ring current, respectively, and N = 0.38 is the current collection efficiency of the platinum ring. Figure 5a,b shows the variation of no. of electron transfer (n) and the H_2O_2 generation on Fe/Fe_3C/FLGs and FLGs. In the potential range between −0.2 and 0.6 V, the n value of Fe/Fe_3C/FLGs is 3.87−3.95, and the H_2O_2 yield remains below 6% which further suggests the preferential $4e^-$ pathway for the ORR process on Fe/Fe_3C/FLGs and is consistent with the K−L analysis.

Figure 5c gives the Tafel slopes which were used to evaluate the ORR kinetic character of the catalyst. The Fe/Fe_3C/FLGs exhibit a smaller Tafel slope (~78.46 mV/dec) than that of the FLGs (~116.44 mV/dec) and are very close to that of the reported commercial state-of-the-art Pt/C electrocatalyst (~76 mV/dec).[38] Besides, EIS tests of Fe/Fe_3C/FLGs and FLG materials were conducted, and the Nyquist plots are displayed in Figure 5d. Obviously, the Fe/Fe_3C/FLG electrode shows lower charge-transfer resistance (R_{ct}) (~73 Ω) as compared to the FLG electrode (~290 Ω). EIS results demonstrate that the introduction of Fe/Fe_3C helps to decrease the charge-transfer resistance, resulting in enhanced electrochemical properties.

Stability is another key parameter that verifies the ORR performance. The LSV curves of FLGs and Fe/Fe_3C/FLGs before and after 1000 potential cycles are shown in Figure 6a. The stability of the FLGs decreased obviously because of the high concentration of H_2O_2 in the continuous test process,[39] resulting in performance degradation. However, the LSV curve after 1000 cycles of Fe/Fe_3C/FLGs almost overlaps with the one before, which demonstrates the excellent stability of the as-prepared Fe/Fe_3C/FLG nanocomposite. The resistance to methanol poisoning for Fe/Fe_3C/FLGs and Pt/C was evaluated in 0.1 M NaOH containing 0.5 M methanol. The relative current (I/I_0) of commercial Pt/C descends steeply and could not be restored to the original state, whereas that of Fe/Fe_3C/FLGs remained essentially unchanged as Figure 6b shows. These results demonstrate that Fe/Fe_3C/FLGs have superior stable electrochemical catalytic activity than the Pt/C catalyst for methanol oxidation, making it high potential to be used in practical devices.

4. CONCLUSIONS

In this work, a Fe/Fe_3C/FLG composite was fabricated through a simple and environmentally friendly approach and exhibited a high-performance ORR electrocatalyst. Multiple characterizations confirm the nanosize of Fe particles with the Fe_3C interface was uniformly distributed on the graphene sheet. Electrocatalytic kinetics investigation of the nanocomposite indicates that the electron transfer process is a four-electron pathway. The formation of a suitable interface of Fe_3C between the Fe nanoparticles and FLGs may promote the electron

https://doi.org/10.1021/acsomega.2c02395
ACS Omega 2022, 7, 25458−25465

transfer process. Furthermore, the Fe/Fe_3C/FLG nanocomposite not only exhibits high ORR catalytic activity but also has very good stability. Consequently, the obtained Fe/Fe_3C/FLG hybrid nanocomposite might be a promising non-precious, cheap, and high-efficiency catalyst for fuel cells.

AUTHOR INFORMATION

Corresponding Author

Hui Zheng − *Laboratory for Nanoelectronics and NanoDevices, Department of Electronics Science and Technology, Hangzhou Dianzi University, Hangzhou 310018, China;* orcid.org/0000-0002-5128-6606; Email: zhenghui0551@hdu.edu.cn

Authors

Meiling Sun − *Laboratory for Nanoelectronics and NanoDevices, Department of Electronics Science and Technology, Hangzhou Dianzi University, Hangzhou 310018, China*

Fangying Yuan − *Laboratory for Nanoelectronics and NanoDevices, Department of Electronics Science and Technology, Hangzhou Dianzi University, Hangzhou 310018, China*

Runqiu Li − *Laboratory for Nanoelectronics and NanoDevices, Department of Electronics Science and Technology, Hangzhou Dianzi University, Hangzhou 310018, China*

Shijun Dong − *Laboratory for Nanoelectronics and NanoDevices, Department of Electronics Science and Technology, Hangzhou Dianzi University, Hangzhou 310018, China*

Ye Zhao − *Laboratory for Nanoelectronics and NanoDevices, Department of Electronics Science and Technology, Hangzhou Dianzi University, Hangzhou 310018, China*

Wenxia Zhong − *Laboratory for Nanoelectronics and NanoDevices, Department of Electronics Science and Technology, Hangzhou Dianzi University, Hangzhou 310018, China*

Chang Shen − *Laboratory for Nanoelectronics and NanoDevices, Department of Electronics Science and Technology, Hangzhou Dianzi University, Hangzhou 310018, China*

Junpeng Wu − *Laboratory for Nanoelectronics and NanoDevices, Department of Electronics Science and Technology, Hangzhou Dianzi University, Hangzhou 310018, China*

Complete contact information is available at: https://pubs.acs.org/10.1021/acsomega.2c02395

Author Contributions

M.S., R.L., and H.Z. conceived and designed the project. F.Y., S.D., and Y.Z. performed the electrochemical experiments and analyzed the electrochemical data. W.Z. and C.S. performed the measurements. M.S. and J.W. analyzed the experimental data. M.S. and H.Z. wrote and edited the manuscript with input from all authors. All authors reviewed and contributed to the manuscript.

Notes

The authors declare no competing financial interest.

ACKNOWLEDGMENTS

This work was funded by the National Natural Science Foundation of China (grant no. 51702075).

REFERENCES

(1) Zhao, Z.; Li, M.; Zhang, L.; Dai, L.; Xia, Z. Design Principles for Heteroatom-Doped Carbon Nanomaterials as Highly Efficient Catalysts for Fuel Cells and Metal-Air Batteries. *Adv. Mater.* **2015**, *27*, 6834.

(2) Jung, N.; Chung, D. Y.; Ryu, J.; Yoo, S. J.; Sung, Y.-E. Pt-based nanoarchitecture and catalyst design for fuel cell applications. *Nano Today* **2014**, *9*, 433.

(3) Xia, W.; Mahmood, A.; Liang, Z.; Zou, R.; Guo, S. Earth-Abundant Nanomaterials for Oxygen Reduction. *Angew. Chem., Int. Ed.* **2016**, *55*, 2650.

(4) Sun, T.; Xu, L.; Wang, D.; Li, Y. Metal Organic Frameworks Derived Single Atom Catalysts for Electrocatalytic Energy Conversion. *Nano Res.* **2019**, *12*, 2067.

(5) Gewirth, A. A.; Varnell, J. A.; DiAscro, A. M. Nonprecious Metal Catalysts for Oxygen Reduction in Heterogeneous Aqueous Systems. *Chem. Rev.* **2018**, *118*, 2313.

(6) Zhang, W.; Lai, W.; Cao, R. Energy-Related Small Molecule Activation Reactions: Oxygen Reduction and Hydrogen and Oxygen Evolution Reactions Catalyzed by Porphyrin- and Corrole-Based Systems. *Chem. Rev.* **2017**, *117*, 3717.

(7) Kulkarni, A.; Siahrostami, S.; Patel, A.; Nørskov, J. K. Understanding Catalytic Activity Trends in the Oxygen Reduction Reaction. *Chem. Rev.* **2018**, *118*, 2302.

(8) Min, M.-k.; Cho, J.; Cho, K.; Kim, H. Particle size and alloying effects of Pt-based alloy catalysts for fuels cell applications. *Electrochim. Acta* **2000**, *45*, 4211.

(9) Bian, W.; Yang, Z.; Strasser, P.; Yang, R. A CoFe2O4/graphene nanohybrid as an efficient bi-functional electrocatalyst for oxygen reduction and oxygen evolution. *J. Power Sources* **2014**, *250*, 196.

(10) Fu, L.; Lu, Y.; Liu, Z.; Zhu, R. Influence of the metal sites of M-N-C (M = Co, Fe, Mn) catalysts derived from metalloporphyrins in ethylbenzene oxidation, Chinese Journal of Catalysis. *Chin. J. Catal.* **2016**, *37*, 398.

(11) Wu, G.; Santandreu, A.; Kellogg, W.; Gupta, S.; Ogoke, O.; Zhang, H.; Wang, H.-L.; Dai, L. Carbon nanocomposite catalysts for oxygen reduction and evolution reactions: From nitrogen doping to transition-metal addition. *Nano Energy* **2016**, *29*, 83.

(12) Shao, M.; Chang, Q.; Dodelet, J.-P.; Chenitz, R. Recent Advances in Electrocatalysts for Oxygen Reduction Reaction. *Chem. Rev.* **2016**, *116*, 3594.

(13) Masa, J.; Xia, W.; Sinev, I.; Zhao, A.; Sun, Z.; Grützke, S.; Weide, P.; Muhler, M.; Schuhmann, W. MnxOy/NC and CoxOy/NC Nanoparticles Embedded in a Nitrogen-Doped Carbon Matrix for High-Performance Bifunctional Oxygen Electrodes. *Angew. Chem., Int. Ed. Engl.* **2014**, *53*, 8508.

(14) Yan, Y.; Cheng, H.; Qu, Z.; Yu, R.; Liu, F.; Ma, Q.; Zhao, S.; Hu, H.; Cheng, Y.; Yang, C.; Li, Z.; Wang, X.; Hao, S.; Chen, Y.; Liu, M. Recent progress on the synthesis and oxygen reduction applications of Fe-based single-atom and double-atom catalysts. *J. Mater. Chem. A* **2021**, *9*, 19489.

(15) Yang, X.-F.; Wang, A.; Qiao, B.; Li, J.; Liu, J.; Zhang, T. Single-atom catalysts: a new frontier in heterogeneous catalysis. *Acc. Chem. Res.* **2013**, *46*, 1740.

(16) Liang, S.; Hao, C.; Shi, Y. The Power of Single-Atom Catalysis. *ChemCatChem* **2015**, *7*, 2559.

(17) Lee, P. M.; Wang, Z.; Liu, X.; Chen, Z.; Liu, E. Glassy carbon electrode modified by graphene−gold nanocomposite coating for detection of trace lead ions in acetate buffer solution. *Thin Solid Films* **2015**, *584*, 85.

(18) Zhu, Y.; Murali, S.; Cai, W.; Li, X.; Suk, J. W.; Potts, J. R.; Ruoff, R. S. Correction: Graphene and Graphene Oxide: Synthesis, Properties, and Applications. *Adv. Mater.* **2010**, *22*, 3906.

(19) Hu, J.; Zheng, J.; Tian, L.; Duan, Y.; Lin, L.; Cui, S.; Peng, H.; Liu, T.; Guo, H.; Wang, X.; Pan, F. A core−shell nanohollow-γ-Fe2O3@graphene hybrid prepared through the Kirkendall process as a high performance anode material for lithium ion batteries. *Chem. Commun.* **2015**, *51*, 7855.

https://doi.org/10.1021/acsomega.2c02395
ACS Omega 2022, 7, 25458−25465

(20) Zaka, A.; Hayat, K.; Mittal, V. Recent Trends in the Use of Three-Dimensional Graphene Structures for Supercapacitors. *ACS Appl. Electron. Mater.* **2021**, *3*, 574.
(21) Eda, G.; Chhowalla, M. Graphene patchwork. *ACS Nano* **2011**, *5*, 4265.
(22) Huang, X.; Qi, X.; Boey, F.; Zhang, H. Graphene-based composites. *Chem. Soc. Rev.* **2012**, *41*, 666.
(23) Geim, A. K. Graphene: status and prospect. *Science* **2009**, *324*, 1530.
(24) Sun, C.; Li, Z.; Zhong, X.; Wang, S.; Yin, X.; Wang, L. Three-Dimensional Graphene-Supported Cobalt Phthalocyanine as Advanced Electrocatalysts for Oxygen Reduction Reaction. *J. Electrochem. Soc.* **2018**, *165*, F24−F31.
(25) Nandan, R.; Gautam, A.; Tripathi, S.; Nanda, K. K. A comprehensive analysis and rational designing of efficient Fe-based oxygen electrocatalysts for metal−air batteries. *J. Mater. Chem. A* **2018**, *6*, 8537.
(26) Wang, X.; Zhang, H.; Lin, H.; Gupta, S.; Wang, C.; Tao, Z.; Fu, H.; Wang, T.; Zheng, J.; Wu, G.; Li, X. Directly converting Fe-doped metal−organic frameworks into highly active and stable Fe-N-C catalysts for oxygen reduction in acid. *Nano Energy* **2016**, *25*, 110.
(27) Li, Y.; Xu, Z.; Sun, X.; Han, J.; Guo, R. Fe, P, N- and FeP, N-doped carbon hollow nanospheres: A comparison study toward oxygen reduction reaction electrocatalysts. *J. Colloid Interface Sci.* **2021**, *602*, 376.
(28) Kramm, U.; Abs-Wurmbach, I.; Herrmann-Geppert, I.; Radnik, J.; Fiechter, S.; Bogdanoffa, P. Influence of the Electron-Density of FeN[sub 4]-Centers Towards the Catalytic Activity of Pyrolyzed FeTMPPCl-Based ORR-Electrocatalysts. *J. Electrochem. Soc.* **2010**, *158*, B69.
(29) Cheon, J. Y.; Kim, J. H.; Kim, J. H.; Goddeti, K. C.; Park, J. Y.; Joo, S. H. Intrinsic Relationship between Enhanced Oxygen Reduction Reaction Activity and Nanoscale Work Function of Doped Carbons. *J. Am. Chem. Soc.* **2014**, *136*, 8875.
(30) Liu, Y.; Li, Z.; Sun, C.; Wang, S.; Wang, L.; Niu, X.; Sun, P.; Zhang, S. Closely packed planar polyphthalocyanine iron/hierarchical three-dimensional graphene as an oxygen electrocatalyst for ORR, OER, and zinc-air battery. *Sustainable Energy Fuels* **2021**, *5*, 5216−5226.
(31) Hu, Y.; Jensen, J. O.; Wei, Z.; Cleemann, L. N.; Xing, W.; Bjerrum, N. J.; Li, Q. Hollow Spheres of Iron Carbide Nanoparticles Encased in Graphitic Layers as Oxygen Reduction Catalysts. *Angew. Chem., Int. Ed.* **2014**, *53*, 3675.
(32) Du, C.; Huang, H.; Feng, X.; Wu, S.; Song, W. Confining MoS2 nanodots in 3D porous nitrogen-doped graphene with amendable ORR performance. *J. Mater. Chem. A* **2015**, *3*, 7616.
(33) Wang, C.; Zhang, H.; Wang, J.; Zhao, Z.; Wang, J.; Zhang, Y.; Cheng, M.; Zhao, H.; Wang, J. Atomic Fe embedded in carbon nanoshells-graphene nanomeshes with enhanced oxygen reduction reaction performance. *Chem. Mater.* **2017**, *29*, 9915.
(34) Xin, D.; Xiao, M.; Yang, R.; Fan, G.; Chen, H.; Ye, H.; Yan, L.; Zhu, C.; Deng, Y.; Zheng, J. The Effect of CNTs on Performance Improvement of rGO Supported Fe-Nx/C Electrocatalysts for the Oxygen Reduction Reaction. *J. Electrochem. Soc.* **2018**, *165*, F401.
(35) Osmieri, L.; Monteverde Videla, A. H. A.; Specchia, S. The use of different types of reduced graphene oxide in the preparation of Fe-N-C electrocatalysts: capacitive behavior and oxygen reduction reaction activity in alkaline medium. *J. Solid State Electrochem.* **2016**, *20*, 3507.
(36) Wang, X.; Du, J.; Zhang, Q.; Gu, L.; Cao, L.; Liang, H.-P. In situ synthesis of sustainable highly efficient single iron atoms anchored on nitrogen doped carbon derived from renewable biomass. *Carbon* **2020**, *157*, 614−621.
(37) Wang, C.; Li, Z.; Wang, L.; Niu, X.; Wang, S. Facile Synthesis of 3D Fe/N Codoped Mesoporous Graphene as Efficient Bifunctional Oxygen Electrocatalysts for Rechargeable Zn-Air Batteries. *ACS Sustainable Chem. Eng.* **2019**, *7*, 13873−13885.
(38) Xu, J.; Lai, S.; Qi, D.; Hu, M.; Peng, X.; Liu, Y.; Liu, W.; Hu, G.; Xu, H.; Li, F.; Li, C.; He, J.; Zhuo, L.; Sun, J.; Qiu, Y.; Zhang, S.; Luo, J.; Liu, X. Atomic Fe-Zn dual-metal sites for high-efficiency PH-universal oxygen reduction catalysis. *Nano Res.* **2021**, *14*, 1374−1381.
(39) Schulenburg, H.; Stankov, S.; Schünemann, V.; Radnik, J.; Dorbandt, I.; Fiechter, S.; Bogdanoff, P.; Tributsch, H. Catalysts for the Oxygen Reduction from Heat-Treated Iron(III) Tetramethoxyphenylporphyrin Chloride: Structure and Stability of Active Sites. *J. Phys. Chem. B* **2003**, *107*, 9034.

https://doi.org/10.1021/acsomega.2c02395
ACS Omega 2022, 7, 25458−25465